Appl. Math. Mech. -Engl. Ed., **39**(9), 1353–1372 (2018)

Applied Mathematics and Mechanics (English Edition)

https://doi.org/10.1007/s10483-018-2369-9

Superconvergence analysis of bi-k-degree rectangular elements for two-dimensional time-dependent Schrödinger equation*

Jianyun WANG[1], Yanping CHEN[2,†]

1. School of Science, Hunan University of Technology, Zhuzhou 412007, Hunan Province, China;

2. School of Mathematical Sciences, South China Normal University, Guangzhou 510631, China

(Received Dec. 13, 2017 / Revised Apr. 20, 2018)

Abstract Superconvergence has been studied for long, and many different numerical methods have been analyzed. This paper is concerned with the problem of superconvergence for a two-dimensional time-dependent linear Schrödinger equation with the finite element method. The error estimate and superconvergence property with order $O(h^{k+1})$ in the H^1 norm are given by using the elliptic projection operator in the semi-discrete scheme. The global superconvergence is derived by the interpolation post-processing technique. The superconvergence result with order $O(h^{k+1}+\tau^2)$ in the H^1 norm can be obtained in the Crank-Nicolson fully discrete scheme.

Key words superconvergence, elliptic projection, Schrödinger equation, interpolation post-processing

Chinese Library Classification O241.82
2010 Mathematics Subject Classification 65M12, 65M15, 65M60

1 Introduction

We shall consider a linear Schrödinger equation as follows. Let $\Omega \subset \mathbb{R}^2$ be a bounded rectangular-type domain with a smooth boundary $\partial\Omega$. We find a complex-valued function $u(\boldsymbol{x},t)$ defined on $\Omega \times [0,T]$ and satisfying

$$\begin{cases} \mathrm{i}u_t(\boldsymbol{x},t) = -\dfrac{1}{2}\Delta u(\boldsymbol{x},t) + V(\boldsymbol{x})u(\boldsymbol{x},t) + f(\boldsymbol{x},t) \quad \text{in} \quad \Omega\times[0,T], \\ u(\boldsymbol{x},t) = 0 \quad \text{on} \quad \partial\Omega\times[0,T], \\ u(\boldsymbol{x},0) = u_0(\boldsymbol{x}) \quad \text{in} \quad \Omega, \end{cases} \tag{1}$$

where $u_0(\boldsymbol{x})$ is a given initial complex-valued function, and the trapping potential function $V(\boldsymbol{x})$ is non-negative bounded and real-valued.

The Schrödinger equation is an important equation in quantum mechanics. There are many numerical methods to solve the Schrödinger equation in the literature, such as the spectral

---

∗ Citation: WANG, J. Y. and CHEN, Y. P. Superconvergence analysis of bi-k-degree rectangular elements for two-dimensional time-dependent Schrödinger equation. *Applied Mathematics and Mechanics* (*English Edition*), **39**(9), 1353–1372 (2018) https://doi.org/10.1007/s10483-018-2369-9

† Corresponding author, E-mail: yanpingchen@scnu.edu.cn

Project supported by the National Natural Science Foundation of China (No. 11671157)

method[1–2], the finite difference method[3–5], the finite element method[6–12], the discontinuous Galerkin method[13–15], and the local discontinuous Galerkin method[16–18]. Bao et al.[1] studied the performance of time-splitting spectral approximations for the general nonlinear Schrödinger equation in the semiclassical regimes. Han et al.[5] introduced an artificial boundary condition to reduce the one-dimensional time-dependent Schrödinger equation into an initial-boundary value problem in a finite computational domain. Antonopoulou et al.[7] considered an initial and boundary-value problem for a general Schrödinger-type equation posed on a two space-dimensional noncylindrical domain with mixed boundary conditions. Karakashian and Makridakis[14] analyzed the convergence of the discontinuous Galerkin method for the nonlinear Schrödinger equation. Guo and Xu[16] presented a fully discrete scheme by discretizing the space with the local discontinuous Galerkin method and the time with the Crank-Nicholson scheme to simulate the multi-dimensional Schrödinger equation with wave operator.

Superconvergence has been studied for long. Many different numerical methods have been analyzed. It is a powerful tool to improve the approximation accuracy and efficiency. There are numerous studies by many famous scholars[19–22]. At present, superconvergence results were obtained widely for elliptic, parabolic, Maxwell's equations, and optimal control problems[23–31]. However, there were not many superconvergence results for the Schrödinger equation[32–36]. In 1998, Lin and Liu[32] studied a time-dependent linear Schrödinger equation and analyzed the superconvergence error results. In 2014, Shi et al.[33] considered a nonlinear Schrödinger equation by the finite element method in the triangular anisotropic meshes and proved the superconvergence result in the semi-discrete scheme. Later, Wang et al.[35] conducted the superconvergence analysis for a time-dependent Schrödinger equation by using the interpolation operator and obtained the error result in the H^1 norm with $O(h^{p+1})$ in the semi-discrete scheme and $O(h^{p+1}+\tau^{\frac{3}{2}})$ in the Crank-Nicolson scheme, respectively. Recently, Zhou et al.[36] studied the superconvergence properties of the local discontinuous Galerkin method for the one-dimensional linear Schrödinger equation.

In this paper, we study a general complex linear Schrödinger equation (1) and extend the previous work[35]. We analyze the error estimate using the elliptic projection operator. We obtain the error result with $O(h^{k+1})$ in the L^2 norm and the H^1 norm in the semi-discrete finite element scheme. The global superconvergence result is presented by use of the interpolation post-processing technique. Next, we analyze the error estimate in the L^2 norm with order $O(h^{k+1}+\tau^2)$ in the Crank-Nicolson fully discrete scheme. We extend the idea[37] and certify that the time-difference of error $\eta^n = U^n - P_h u^n$ has a high order error in the L^2 norm, that is, $\|\eta^n - \eta^{n-1}\| \leqslant C\tau(h^{k+1}+\tau^2)$, where U^n is the fully discrete solution of Crank-Nicolson scheme. At last, we obtain the superconvergence result in the H^1 norm with $O(h^{k+1}+\tau^2)$ on this basis.

The paper is organized as follows. The notations and the projection operator are given in Section 2. In Section 3, we present a finite element semi-discrete scheme with bi-k-degree rectangular elements. Furthermore, we obtain error results with $O(h^{k+1})$ in the L^2 norm and the H^1 norm by use of the elliptic projection operator, respectively. In Section 4, we prove the global superconvergence result with $O(h^{k+1})$. In Section 5, we obtain the superconvergence result in the H^1 norm with $O(h^{k+1}+\tau^2)$ in the Crank-Nicolson fully discrete scheme. In Section 6, numerical examples are given to partly verify the theoretical results.

2 Notation and preliminaries

For an integer $m \geqslant 0$ and $1 \leqslant p \leqslant \infty$, we shall use $W^{m,p}$ to denote the standard Sobolev space of complex-valued measurable functions defined on Ω with the norm $\|\phi\|_{m,p}^p = \sum\limits_{|\alpha|\leqslant m} \|D^\alpha \phi\|_{L^p(\Omega)}^p$. When $p=2$, we shall also use the symbol H^m for $W^{m,2}$, $\|\cdot\|_m$ instead of $\|\cdot\|_{m,2}$, and $\|\cdot\|$ instead of $\|\cdot\|_{0,2}$.

For complex-valued functions $\omega(\boldsymbol{x})$ and $\nu(\boldsymbol{x})$, we define the inner product (ω,ν) with

$$(\omega,\nu)=\int_\Omega \omega(\boldsymbol{x})\overline{\nu}(\boldsymbol{x})\mathrm{d}\boldsymbol{x},$$

where $\overline{\nu}$ denotes the complex conjugate of function ν.

Then, we can define the weak solution $u(\boldsymbol{x},t)$ of problem (1): find a function $u(\boldsymbol{x},t)\in H_0^1(\Omega)$ such that

$$\begin{cases} \mathrm{i}(u_t,v)=a(u,v)+(f,v), \quad \forall v\in H_0^1(\Omega), \quad 0\leqslant t\leqslant T,\\ u(\boldsymbol{x},0)=u_0(\boldsymbol{x}), \quad \forall \boldsymbol{x}\in\Omega, \end{cases} \tag{2}$$

where $a(u,v)=\frac{1}{2}(\nabla u,\nabla v)+(Vu,v)$.

Let Γ_h be a quasi-uniform rectangular partition of Ω with the mesh size $h>0$, and let e be an arbitrary element of Γ_h. We can define the finite element space of order k as

$$V^{h,k}=\{v\in C(\Omega): v|_e\in Q_p, \quad \forall e\in\Gamma_h\},$$

where

$$Q_p=\mathrm{span}\{x^iy^j, \quad 0\leqslant i,j\leqslant k\}.$$

In addition,

$$V_0^{h,k}=V^{h,k}\cap H_0^1(\Omega).$$

Let $V_0^{h,k}\subset H_0^1(\Omega)$ be the corresponding finite element space of order k. In general given $w(\boldsymbol{x},t)\in H_0^1(\Omega)$, the elliptic projection $P_hw(\boldsymbol{x},t)\in V_0^{h,k}$ can be defined by

$$a(P_hw,v_h)=a(w,v_h), \quad \forall v_h\in V_0^{h,k}. \tag{3}$$

Let $\tau=T/N$ be the time step of the interval $[0,T]$, time nodes $t_j=j\tau$ $(j=0,1,\cdots,N)$, $t_{j+\frac{1}{2}}=(t_{j+1}+t_j)/2$, and time elements $I_j=[t_j,t_{j+1}]$ $(j=0,1,\cdots,N-1)$, and set

$$\begin{aligned} &\phi(\cdot,t_j)=\phi^j,\\ &\|\phi\|_{L^2(0,T;\Omega)}=\Big(\int_0^T\|\phi(\cdot,t)\|_\Omega^2\mathrm{d}t\Big)^{\frac{1}{2}}. \end{aligned}$$

3 Superconvergence analysis for semi-discrete approximation problem

The semi-discrete finite element solution $u_h(\boldsymbol{x},t)$ of problem (1) can be defined: find $u_h(\boldsymbol{x},t)\in V_0^{h,k}$ satisfying

$$\begin{cases} \mathrm{i}(u_{ht},v_h)=a(u_h,v_h)+(f,v_h), \quad \forall v_h\in V_0^{h,k}, \quad 0\leqslant t\leqslant T,\\ u_h(\boldsymbol{x},0)=P_hu_0(\boldsymbol{x}), \quad \forall \boldsymbol{x}\in\Omega, \end{cases} \tag{4}$$

where $P_hu_0(\boldsymbol{x})\in V_0^{h,k}$ is the elliptic projection of $u_0(\boldsymbol{x})$.

Lemma 1[34] *If for any $t\in[0,T]$, the functions $u(\boldsymbol{x},t),u_t(\boldsymbol{x},t),u_{tt}(\boldsymbol{x},t)\in H^{k+1}(\Omega)$, then $P_hu(\boldsymbol{x},t)\in V_0^{h,k}$ has the following results*:

$$\|u-P_hu\|_q\leqslant Ch^{k-q+1}\|u\|_{k+1}, \quad q=0,1, \tag{5}$$

$$\|(u-P_hu)_t\|_q\leqslant Ch^{k-q+1}\|u_t\|_{k+1}, \quad q=0,1, \tag{6}$$

$$\|(u-P_hu)_{tt}\|_q\leqslant Ch^{k-q+1}\|u_{tt}\|_{k+1}, \quad q=0,1. \tag{7}$$

Lemma 2[20] *Let u be the solution to the problem* (2), *and let $u_I \in V_0^{h,k}$ be the interpolation of u. If $u \in H^{k+2}(\Omega)$, then*

$$|(\nabla(u - u_I), \nabla v)| \leqslant Ch^{k+1}\|u\|_{k+2}\|v\|_1, \quad \forall v \in V_0^{h,k}. \tag{8}$$

Theorem 1 *If u and u_h are the solutions to the problems* (2) *and* (4), *respectively, and $u, u_t, u_{tt} \in H^{k+1}(\Omega)$, there hold*

$$\|u_h - P_h u\| \leqslant Ch^{k+1}, \tag{9}$$

$$\|(u_h - P_h u)_t\| \leqslant Ch^{k+1}. \tag{10}$$

Proof It follows from (2) and (4) that

$$\mathrm{i}((u - u_h)_t, v_h) = a(u - u_h, v_h), \quad \forall v_h \in V_0^{h,k}. \tag{11}$$

Let $u - u_h = \rho - \xi$ with

$$\rho = u - P_h u, \quad \xi = u_h - P_h u. \tag{12}$$

Then, from (11) and (12), we have

$$\mathrm{i}(\rho_t, v_h) - \mathrm{i}(\xi_t, v_h) = a(\rho, v_h) - a(\xi, v_h). \tag{13}$$

From (3), we can obtain

$$a(\rho, v_h) = 0. \tag{14}$$

Substituting (14) into (13) yields

$$\mathrm{i}(\xi_t, v_h) = \mathrm{i}(\rho_t, v_h) + a(\xi, v_h). \tag{15}$$

Taking $v_h = \xi$ in (15), we have

$$\mathrm{i}(\xi_t, \xi) = \mathrm{i}(\rho_t, \xi) + a(\xi, \xi). \tag{16}$$

Noticing

$$\frac{1}{2}\frac{\mathrm{d}}{\mathrm{d}t}\|\xi\|^2 = \mathrm{Re}\{(\xi_t, \xi)\}$$

and comparing the imaginary parts of (16), we get

$$\begin{aligned}\frac{1}{2}\frac{\mathrm{d}}{\mathrm{d}t}\|\xi\|^2 &= \mathrm{Re}\{(\rho_t, \xi)\} + \mathrm{Im}\{a(\xi, \xi)\} \\ &= \mathrm{Re}\{(\rho_t, \xi)\} \\ &\leqslant C\|\rho_t\|\|\xi\|.\end{aligned} \tag{17}$$

Combining (6) with (17) yields

$$\frac{\mathrm{d}}{\mathrm{d}t}\|\xi\| \leqslant Ch^{k+1}\|u_t\|_{k+1}. \tag{18}$$

Integrating from 0 to t in (18), we have

$$\|\xi\| \leqslant \|\xi(\cdot, 0)\| + Ch^{k+1}\int_0^t \|u_t\|_{k+1}\mathrm{d}s. \tag{19}$$

It follows from (4) that

$$\|\xi(\cdot,0)\| = 0. \tag{20}$$

From (19) and (20), we obtain

$$\|\xi\| \leqslant Ch^{k+1}\int_0^t \|u_t\|_{k+1}\mathrm{d}s.$$

Therefore, (9) holds. Next, we prove (10). Taking $v_h = \xi_t(\cdot,0)$ in (15) with $t = 0$ and combining (20), we have

$$\mathrm{i}(\xi_t(\cdot,0), \xi_t(\cdot,0)) = \mathrm{i}(\rho_t(\cdot,0), \xi_t(\cdot,0)).$$

Thus,

$$\|\xi_t(\cdot,0)\|^2 \leqslant \|\rho_t(\cdot,0)\|\|\xi_t(\cdot,0)\|,$$

that is,

$$\|\xi_t(\cdot,0)\| \leqslant \|\rho_t(\cdot,0)\|. \tag{21}$$

Combining (6) with (21) gives

$$\|\xi_t(\cdot,0)\| \leqslant Ch^{k+1}\|u_t(\cdot,0)\|_{k+1}. \tag{22}$$

Differentiating (15) with respect to t and taking $v_h = \xi_t$, we can obtain

$$\mathrm{i}(\xi_{tt}, \xi_t) = \mathrm{i}(\rho_{tt}, \xi_t) + a(\xi_t, \xi_t). \tag{23}$$

Noticing

$$\frac{1}{2}\frac{\mathrm{d}}{\mathrm{d}t}\|\xi_t\|^2 = \mathrm{Re}\{(\xi_{tt}, \xi_t)\}$$

and comparing the imaginary parts of (23) yield

$$\begin{aligned}\frac{1}{2}\frac{\mathrm{d}}{\mathrm{d}t}\|\xi_t\|^2 &= \mathrm{Re}\{(\rho_{tt}, \xi_t)\} + \mathrm{Im}\{a(\xi_t, \xi_t)\}\\ &= \mathrm{R}e\{(\rho_{tt}, \xi_t)\}\\ &\leqslant C\|\rho_{tt}\|\|\xi_t\|.\end{aligned} \tag{24}$$

From (22) and (25), we get

$$\frac{\mathrm{d}}{\mathrm{d}t}\|\xi_t\| \leqslant Ch^{k+1}\|u_{tt}\|_{k+1}. \tag{25}$$

Integrating from 0 to t in (25), we can obtain

$$\|\xi_t\| \leqslant \|\xi_t(\cdot,0)\| + Ch^{k+1}\int_0^t \|u_{tt}\|_{k+1}\mathrm{d}s. \tag{26}$$

It follows from (22) and (26) that

$$\|\xi_t\| \leqslant Ch^{k+1}\Big(\|u_t(\cdot,0)\|_{k+1} + \int_0^t \|u_{tt}\|_{k+1}\mathrm{d}s\Big),$$

which completes the proof of (10).

Theorem 2 *Let u and u_h be the solutions to the problems* (2) *and* (4), *respectively, and* $u, u_t, u_{tt} \in H^{k+1}(\Omega)$. *Then, we have*

$$\|u_h - P_h u\|_1 \leqslant Ch^{k+1}. \tag{27}$$

Proof Taking $v_h = \xi_t$ in (15), we can get

$$\mathrm{i}(\xi_t, \xi_t) = \mathrm{i}(\rho_t, \xi_t) + a(\xi, \xi_t),$$

that is,

$$\mathrm{i}(\xi_t, \xi_t) = \mathrm{i}(\rho_t, \xi_t) + \frac{1}{2}(\nabla\xi, \nabla\xi_t) + (V\xi, \xi_t). \tag{28}$$

Noticing

$$\frac{1}{2}\frac{\mathrm{d}}{\mathrm{d}t}\|\nabla\xi\|^2 = \mathrm{Re}\{(\nabla\xi, \nabla\xi_t)\}$$

and comparing the real parts of (28) give

$$\begin{aligned}\frac{1}{2}\frac{\mathrm{d}}{\mathrm{d}t}\|\nabla\xi\|^2 &= \mathrm{Im}\{(\rho_t, \xi_t) + (\xi_t, \xi_t)\} - \mathrm{Re}\{(V\xi, \xi_t)\}\\ &= \mathrm{Im}\{(\rho_t, \xi_t)\} - \mathrm{Re}\{(V\xi, \xi_t)\}\\ &\leqslant C(\|\rho_t\| + \|\xi\|)\|\xi_t\|.\end{aligned} \tag{29}$$

From (6), (9), (10), and (29), we can obtain

$$\frac{\mathrm{d}}{\mathrm{d}t}\|\nabla\xi\|^2 \leqslant Ch^{2k+2}. \tag{30}$$

Integrating from 0 to t in (30) yields

$$\|\nabla\xi\|^2 \leqslant \|\nabla\xi(\cdot, 0)\|^2 + Ch^{2k+2}. \tag{31}$$

Notice

$$\|\nabla\xi(\cdot, 0)\| = 0. \tag{32}$$

Substituting (32) into (31) yields

$$\|\nabla\xi\| \leqslant Ch^{k+1}. \tag{33}$$

Therefore, (27) follows from (33).

4 Global superconvergence analysis

Let $\widetilde{e}$ be a macro element which is the union of four elements $e_i \in \Gamma_h$ $(i = 1, 2, 3, 4)$, where the intersection of $\overline{e}_i \in \Gamma_h$ $(i = 1, 2, 3, 4)$ is nonempty (see Fig. 1).

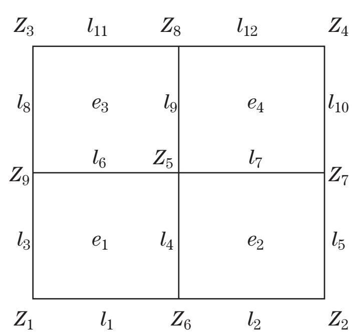

Fig. 1 Structure of macro element $\widetilde{e}$

Let the interpolation operator Π_{2h}^2 satisfy $\Pi_{2h}^2 w \in Q_2(\widetilde{e})$, where Q_2 is the space of bi-quadratic functions, and

$$\Pi_{2h}^2 w(Z_i) = w(Z_i), \tag{34}$$

where Z_i $(i = 1, 2, \cdots, 9)$ are the nodes of Γ_h.

When $k \geqslant 2$, let $\Pi_{2h}^{2k} w \in Q_{2k}(\widetilde{e})$ such that

$$\Pi_{2h}^{2k} w(Z_i) = w(Z_i), \tag{35}$$

$$\int_{l_i} (\Pi_{2h}^{2k} w - w) v \mathrm{d}l = 0, \quad \forall v \in P_{k-2}(l_i), \tag{36}$$

$$\int_{e_i} (\Pi_{2h}^{2k} w - w) v \mathrm{d}x \mathrm{d}y = 0, \quad \forall v \in Q_{k-2}(e_i), \tag{37}$$

where $Z_i\, (i = 1, 2, \cdots, 9)$ are the nodes of Γ_h, $l_i\, (i = 1, 2, \cdots, 12)$ are the edges of Γ_h, $e_i\, (i = 1, 2, 3, 4)$ are the elements of Γ_h, P_{k-2} is the set of polynomials of order $k-2$, and $Q_{k-2}(\widetilde{e})$ is the polynomials of order $k-2$ in x and y.

Lemma 3[20,22] *The interpolation operator Π_{2h}^{2k} is defined in* (34)–(37) *such that*

$$\Pi_{2h}^{2k} w_I = \Pi_{2h}^{2k} w, \quad \forall w \in C(\widetilde{e}), \tag{38}$$

$$\|\Pi_{2h}^{2k} w - w\|_{l,\widetilde{e}} \leqslant C h^{r+1-l} \|w\|_{r+1,\widetilde{e}}, \quad 1 \leqslant r \leqslant 2k, \quad l = 0, 1, \tag{39}$$

$$\|\Pi_{2h}^{2k} v\|_{l,\widetilde{e}} \leqslant C \|v\|_{l,\widetilde{e}}, \quad \forall v \in V^{h,k}, \quad l = 0, 1, \tag{40}$$

where $w_I \in V^{h,k}$ is the interpolant of w.

Lemma 4 *Let u and u_h be the solutions to the problems* (2) *and* (4), *respectively. If $u \in H^{k+2}(\Omega)$, and $u_t, u_{tt} \in H^{k+1}(\Omega)$, then*

$$\|u_h - u_I\|_1 \leqslant C h^{k+1}, \tag{41}$$

where u_I is the interpolant of u.

Proof From (14), we can obtain

$$a(u - P_h u, u_h - u_I) = 0,$$

that is,

$$(\nabla(u - P_h u), \nabla(u_h - u_I)) = -(V(u - P_h u), u_h - u_I). \tag{42}$$

It is easy to check

$$\begin{aligned}(\nabla(u_h - u_I), \nabla(u_h - u_I)) &= (\nabla(u_h - P_h u), \nabla(u_h - u_I)) - (\nabla(u - P_h u), \nabla(u_h - u_I)) \\ &\quad + (\nabla(u - u_I), \nabla(u_h - u_I)).\end{aligned} \tag{43}$$

Combining (42) with (43) yields

$$\begin{aligned}|u_h - u_I|_1^2 &= (\nabla(u_h - P_h u), \nabla(u_h - u_I)) + (V(u - P_h u), u_h - u_I) \\ &\quad + (\nabla(u - u_I), \nabla(u_h - u_I)) \\ &\leqslant \|u_h - P_h u\|_1 \|u_h - u_I\|_1 + C\|u - P_h u\| \|u_h - u_I\| \\ &\quad + (\nabla(u - u_I), \nabla(u_h - u_I)).\end{aligned} \tag{44}$$

It follows from (5) that

$$\|u - P_h u\| \leqslant Ch^{k+1}\|u\|_{k+1}, \tag{45}$$

and from (8), we have

$$(\nabla(u - u_I), \nabla(u_h - u_I)) \leqslant Ch^{k+1}\|u\|_{k+2}\|u_h - u_I\|_1. \tag{46}$$

In addition,

$$\|u_h - u_I\| \leqslant \|u_h - u_I\|_1. \tag{47}$$

Substituting (27) and (45)–(47) into (44), we can get

$$|u_h - u_I|_1^2 \leqslant C(h^{k+1} + h^{k+1}\|u\|_{k+1} + h^{k+1}\|u\|_{k+2})\|u_h - u_I\|_1. \tag{48}$$

By the Poincaré inequality, we can obtain

$$\|u_h - u_I\|_1 \leqslant C|u_h - u_I|_1. \tag{49}$$

Therefore, (48) and (49) show the validity of (41).

Theorem 3 *Let u and u_h be the solutions to the problems* (2) *and* (4), *respectively. If $u \in H^{k+2}(\Omega)$, and $u_t, u_{tt} \in H^{k+1}(\Omega)$, then*

$$\|u - \Pi_{2h}^{2k}u_h\|_1 \leqslant Ch^{k+1}, \tag{50}$$

where Π_{2h}^{2k} is the interpolation post-processing operator.

Proof It follows from (40) and (41) that

$$\|\Pi_{2h}^{2k}u_h - \Pi_{2h}^{2k}u_I\|_1 \leqslant C\|u_h - u_I\|_1 \leqslant Ch^{k+1}. \tag{51}$$

From (38) and (39), we have

$$\|\Pi_{2h}^{2k}u_I - u\|_1 = \|\Pi_{2h}^{2k}u - u\|_1 \leqslant Ch^{k+1}. \tag{52}$$

Notice

$$\|u - \Pi_{2h}^{2k}u_h\|_1 \leqslant \|\Pi_{2h}^{2k}u_h - \Pi_{2h}^{2k}u_I\|_1 + \|\Pi_{2h}^{2k}u_I - u\|_1. \tag{53}$$

Therefore, (50) follows from (51)–(53).

5 Superconvergence analysis in fully discrete scheme

For the function series $U^n(\boldsymbol{x})$ $(n = 0, 1, \cdots)$, let

$$\partial_t U^{n+\frac{1}{2}} = \frac{1}{\tau}(U^{n+1}(\boldsymbol{x}) - U^n(\boldsymbol{x})),$$
$$U^{n+\frac{1}{2}} = \frac{1}{2}(U^{n+1}(\boldsymbol{x}) + U^n(\boldsymbol{x})).$$

Then, the Crank-Nicolson fully discrete finite element solution $U^n(\boldsymbol{x}) \in V_0^{h,k}$ $(n = 0, 1, \cdots, N)$ to the problem (1) can be defined by

$$\begin{cases} \mathrm{i}(\partial_t U^{n+\frac{1}{2}}, v_h) = a(U^{n+\frac{1}{2}}, v_h) + (f^{n+\frac{1}{2}}, v_h), \quad \forall v_h \in V_0^{h,k}, \\ U^0(\boldsymbol{x}) = P_h u_0(\boldsymbol{x}). \end{cases} \tag{54}$$

Theorem 4 *Let $u(\boldsymbol{x},t)$ be the solution to the problem* (2), *and let the function series $U^n(\boldsymbol{x})$ be the solution to the problem* (54). *Then, we have*

$$\|U^n - P_h u^n\| \leqslant Ch^{k+1} + C\tau^2. \tag{55}$$

Proof From (2) and (54), we can get

$$\mathrm{i}(u_t^{n+\frac{1}{2}} - \partial_t U^{n+\frac{1}{2}}, v_h) = a(u^{n+\frac{1}{2}} - U^{n+\frac{1}{2}}, v_h). \tag{56}$$

Let $u - U = \rho - \eta$ with

$$\rho = u - P_h u, \quad \eta = U - P_h u. \tag{57}$$

Combining (56) with (57) and (14), we have

$$\mathrm{i}(\partial_t \eta^{n+\frac{1}{2}}, v_h) - \mathrm{i}(\partial_t \rho^{n+\frac{1}{2}}, v_h) - \mathrm{i}(u_t^{n+\frac{1}{2}} - \partial_t u^{n+\frac{1}{2}}, v_h) = a(\eta^{n+\frac{1}{2}}, v_h). \tag{58}$$

Taking $v_h = \eta^{n+\frac{1}{2}}$ in (58), we can obtain

$$\mathrm{i}(\partial_t \eta^{n+\frac{1}{2}}, \eta^{n+\frac{1}{2}}) - \mathrm{i}(\partial_t \rho^{n+\frac{1}{2}}, \eta^{n+\frac{1}{2}}) - \mathrm{i}(u_t^{n+\frac{1}{2}} - \partial_t u^{n+\frac{1}{2}}, \eta^{n+\frac{1}{2}}) = a(\eta^{n+\frac{1}{2}}, \eta^{n+\frac{1}{2}}). \tag{59}$$

Notice

$$\frac{1}{2\tau}(\|\eta^{n+1}\|^2 - \|\eta^n\|^2) = \mathrm{Re}\{(\partial_t \eta^{n+\frac{1}{2}}, \eta^{n+\frac{1}{2}})\}.$$

Comparing the imaginary parts of (59) yields

$$\begin{aligned}
\frac{1}{2\tau}(\|\eta^{n+1}\|^2 - \|\eta^n\|^2) &= \mathrm{Re}\{(\partial_t \rho^{n+\frac{1}{2}}, \eta^{n+\frac{1}{2}}) + (u_t^{n+\frac{1}{2}} - \partial_t u^{n+\frac{1}{2}}, \eta^{n+\frac{1}{2}})\} \\
&\leqslant |(\partial_t \rho^{n+\frac{1}{2}}, \eta^{n+\frac{1}{2}})| + |(u_t^{n+\frac{1}{2}} - \partial_t u^{n+\frac{1}{2}}, \eta^{n+\frac{1}{2}})| \\
&\leqslant (\|\partial_t \rho^{n+\frac{1}{2}}\| + \|u_t^{n+\frac{1}{2}} - \partial_t u^{n+\frac{1}{2}}\|)\|\eta^{n+\frac{1}{2}}\| \\
&= \frac{1}{2}(\|\partial_t \rho^{n+\frac{1}{2}}\| + \|u_t^{n+\frac{1}{2}} - \partial_t u^{n+\frac{1}{2}}\|)\|\eta^{n+1} + \eta^n\| \\
&\leqslant \frac{1}{2}(\|\partial_t \rho^{n+\frac{1}{2}}\| + \|u_t^{n+\frac{1}{2}} - \partial_t u^{n+\frac{1}{2}}\|)(\|\eta^{n+1}\| + \|\eta^n\|).
\end{aligned}$$

Thus,

$$\|\eta^{n+1}\| - \|\eta^n\| \leqslant C\tau(\|\partial_t \rho^{n+\frac{1}{2}}\| + \|u_t^{n+\frac{1}{2}} - \partial_t u^{n+\frac{1}{2}}\|). \tag{60}$$

It follows from (5) that

$$\begin{aligned}
\|\partial_t \rho^{n+\frac{1}{2}}\| &= \|\partial_t u^{n+\frac{1}{2}} - \partial_t P_h u^{n+\frac{1}{2}}\| \\
&= \|\tau^{-1}(u^{n+1} - u^n) - \tau^{-1}(P_h u^{n+1} - P_h u^n)\| \\
&= \tau^{-1}\|(u^{n+1} - u^n) - P_h(u^{n+1} - u^n)\| \\
&\leqslant C\tau^{-1}h^{k+1}\|u^{n+1} - u^n\|_{k+1} \\
&= C\tau^{-1}h^{k+1}\Big\|\int_{t_n}^{t_{n+1}} u_t(\cdot,t)\Big\|_{k+1}\mathrm{d}t \\
&\leqslant C\tau^{-1}h^{k+1}\int_{t_n}^{t_{n+1}} \|u_t(\cdot,t)\|_{k+1}\mathrm{d}t.
\end{aligned} \tag{61}$$

In addition,

$$
\begin{aligned}
&\|u_t^{n+\frac{1}{2}} - \partial_t u^{n+\frac{1}{2}}\| \\
&= \frac{1}{2\tau}\Big\| \int_{t_n}^{t_{n+\frac{1}{2}}} (t-t_n)^2 u_{ttt}(\cdot,t)\mathrm{d}t + \int_{t_{n+\frac{1}{2}}}^{t_{n+1}} (t-t_{n+1})^2 u_{ttt}(\cdot,t)\mathrm{d}t\Big\| \\
&\leqslant \frac{1}{2\tau}\Big\| \int_{t_n}^{t_{n+\frac{1}{2}}} \Big(\frac{\tau}{2}\Big)^2 u_{ttt}(\cdot,t)\mathrm{d}t + \int_{t_{n+\frac{1}{2}}}^{t_{n+1}} \Big(\frac{\tau}{2}\Big)^2 u_{ttt}(\cdot,t)\mathrm{d}t\Big\| \\
&= \frac{\tau}{8}\Big\| \int_{t_n}^{t_{n+1}} u_{ttt}(\cdot,t)\mathrm{d}t\Big\| \\
&\leqslant C\tau \int_{t_n}^{t_{n+1}} \|u_{ttt}(\cdot,t)\|\mathrm{d}t.
\end{aligned} \tag{62}
$$

Substituting (61) and (62) into (60), we have

$$
\begin{aligned}
\|\eta^{n+1}\| - \|\eta^n\| \leqslant{}& Ch^{k+1} \int_{t_n}^{t_{n+1}} \|u_t(\cdot,t)\|_{k+1}\mathrm{d}t \\
&+ C\tau^2 \int_{t_n}^{t_{n+1}} \|u_{ttt}(\cdot,t)\|\mathrm{d}t.
\end{aligned} \tag{63}
$$

Summing up for n in (63) yields

$$
\begin{aligned}
\|\eta^{n}\| - \|\eta^0\| \leqslant{}& Ch^{k+1} \int_{0}^{t_{n}} \|u_t(\cdot,t)\|_{k+1}\mathrm{d}t \\
&+ C\tau^2 \int_{0}^{t_{n}} \|u_{ttt}(\cdot,t)\|\mathrm{d}t.
\end{aligned} \tag{64}
$$

From (54), we can see

$$
\|\eta^0\| = 0. \tag{65}
$$

Therefore, (55) follows from (64) and (65).

Lemma 5 *Let $u(\boldsymbol{x},t)$ be the solution to the problem* (2), *and let the function series $U^n(\boldsymbol{x})$ be the solution to the problem* (54). *Then, the time-difference of error $\eta^n = U^n - P_h u^n$ has a high order error*

$$
\|\eta^n - \eta^{n-1}\| \leqslant C\tau(h^{k+1} + \tau^2). \tag{66}
$$

Proof It follows from (2) that

$$
\int_0^t (\mathrm{i}(u_t,v) - a(u,v) - (f,v))\mathrm{d}t = 0, \quad \forall v \in V_0^{h,k}. \tag{67}
$$

Integrating (67) in I_n by trapezoid and mid-point formulae, respectively, we can obtain

$$
\mathrm{i}(u^{n+1} - u^n, v) - \frac{\tau}{2} a(u^{n+1} + u^n, v) = \tau(f^{n+\frac{1}{2}}, v) + r_1^n(v) + r_2^n(v), \tag{68}
$$

where

$$
r_1^n(v) = O(\tau^2) \int_{I_n} \|f_{tt}\|\|v\|\mathrm{d}t, \tag{69}
$$

$$
r_2^n(v) = O(\tau^2) \int_{I_n} (\|u_{tt}\|_2 + \|V u_{tt}\|)\|v\|\mathrm{d}t. \tag{70}
$$

From (54), we have

$$\mathrm{i}(U^{n+1}-U^n,v)-\frac{\tau}{2}a(U^{n+1}+U^n,v)=\tau(f^{n+\frac{1}{2}},v). \tag{71}$$

Combining (68) with (71) yields

$$\begin{aligned}&\mathrm{i}(u^{n+1}-U^{n+1}-(u^n-U^n),v)-\frac{\tau}{2}a(u^{n+1}-U^{n+1}+u^n-U^n,v)\\&=r_1^n(v)+r_2^n(v).\end{aligned} \tag{72}$$

From (57), (14), and (72), we get

$$\mathrm{i}(\eta^{n+1}-\eta^n,v)-\frac{\tau}{2}a(\eta^{n+1}+\eta^n,v)=r_1^n(v)+r_2^n(v)+r_3^n(v), \tag{73}$$

where

$$r_3^n(v)=\mathrm{i}(\rho^{n+1}-\rho^n,v)=\mathrm{i}\int_{I_n}(\rho_t,v)\mathrm{d}t. \tag{74}$$

Further, combining (7) and (74) gives

$$\begin{aligned}|r_3^n(v)-r_3^{n-1}(v)|&=\Big|\int_{I_n}(\rho_t,v)\mathrm{d}t-\int_{I_{n-1}}(\rho_t,v)\mathrm{d}t\Big|\\&=O(\tau)\int_{I_n+I_{n-1}}|(\rho_{tt},v)|\mathrm{d}t\\&=O(\tau h^{k+1})\int_{I_n+I_{n-1}}\|u_{tt}\|_{k+1}\|v\|\mathrm{d}t.\end{aligned} \tag{75}$$

Substituting n by $n-1$ in (73), we have

$$\mathrm{i}(\eta^n-\eta^{n-1},v)-\frac{\tau}{2}a(\eta^n+\eta^{n-1},v)=r_1^{n-1}(v)+r_2^{n-1}(v)+r_3^{n-1}(v). \tag{76}$$

Let

$$\epsilon^{n+1}=\eta^{n+1}-\eta^n.$$

We can see

$$(\eta^{n+1}+\eta^n)-(\eta^n+\eta^{n-1})=\epsilon^{n+1}+\epsilon^n. \tag{77}$$

Subtracting (76) from (73) and combining (77) yield

$$\mathrm{i}(\epsilon^{n+1}-\epsilon^n,v)-\frac{\tau}{2}a(\epsilon^{n+1}+\epsilon^n,v)=r_h^n(v), \tag{78}$$

where

$$r_h^n(v)=\sum_{i=1}^{3}(r_i^n(v)-r_i^{n-1}(v)). \tag{79}$$

From (69), (70), (75), and (79), we can obtain

$$\begin{aligned}|r_h^n(v)|&\leqslant\sum_{i=1}^{3}|r_i^n(v)-r_i^{n-1}(v)|\\&\leqslant C\tau(h^{k+1}+\tau^2)\int_{I_n+I_{n-1}}(\|f_{ttt}\|+\|u_{ttt}\|_2\\&\quad+\|Vu_{ttt}\|+\|u_{tt}\|_{k+1})\|v\|\mathrm{d}t.\end{aligned} \tag{80}$$

Taking $v=\epsilon^{n+1}+\epsilon^n$ in (78), we get

$$\mathrm{i}(\epsilon^{n+1}-\epsilon^n,\epsilon^{n+1}+\epsilon^n)-\frac{\tau}{2}a(\epsilon^{n+1}+\epsilon^n,\epsilon^{n+1}+\epsilon^n)=r_h^n(\epsilon^{n+1}+\epsilon^n). \tag{81}$$

Comparing the imaginary parts of (81), we have

$$\begin{aligned}\|\epsilon^n\|^2-\|\epsilon^{n-1}\|^2&=\mathrm{Re}\{(\epsilon^{n+1}-\epsilon^n,\epsilon^{n+1}+\epsilon^n)\}\\&=\mathrm{Im}\{r_h^n(\epsilon^{n+1}+\epsilon^n)\}\\&\leqslant|r_h^n(\epsilon^{n+1}+\epsilon^n)|.\end{aligned} \tag{82}$$

Combining (80) with (82) gives

$$\begin{aligned}\|\epsilon^n\|^2-\|\epsilon^{n-1}\|^2\leqslant C\tau(h^{k+1}+\tau^2)\int_{I_n+I_{n-1}}&(\|f_{ttt}\|+\|u_{ttt}\|_2\\&+\|Vu_{ttt}\|+\|u_{tt}\|_{k+1})\|\epsilon^{n+1}+\epsilon^n\|\mathrm{d}t.\end{aligned} \tag{83}$$

Without loss of generality, we assume that there is an integer $1\leqslant K\leqslant N$ such that

$$\|\epsilon^K\|=\max_{1\leqslant n\leqslant N}\|\epsilon^n\|. \tag{84}$$

Summing up for n from 2 to K in (83) and combining (84), we have

$$\begin{aligned}\|\epsilon^K\|^2\leqslant\|\epsilon^1\|^2+C\tau(h^{k+1}+\tau^2)\int_I&(\|f_{ttt}\|+\|u_{ttt}\|_2\\&+\|Vu_{ttt}\|+\|u_{tt}\|_{k+1})\mathrm{d}t\|\epsilon^K\|.\end{aligned} \tag{85}$$

Taking $n=1$ in (64) and combining (65) yield

$$\|\epsilon^1\|=\|\eta^1\|\leqslant C\tau(h^{k+1}+\tau^2). \tag{86}$$

Substituting (86) into (85) and using Young's inequality, we can get

$$\|\epsilon^K\|\leqslant C\tau(h^{k+1}+\tau^2). \tag{87}$$

Therefore, (66) follows from (84) and (87).

Theorem 5 *Let $u(\boldsymbol{x},t)$ be the solution to the problem* (2), *and let the function series $U^n(\boldsymbol{x})$ be the solution to the problem* (54). *Then, we have*

$$\|U^n-P_hu^n\|_1\leqslant Ch^{k+1}+C\tau^2. \tag{88}$$

Proof Taking $v_h=\partial_t\eta^{n+\frac12}$ in (58), we have

$$\begin{aligned}&\mathrm{i}(\partial_t\eta^{n+\frac12},\partial_t\eta^{n+\frac12})-\mathrm{i}(\partial_t\rho^{n+\frac12},\partial_t\eta^{n+\frac12})-\mathrm{i}(u_t^{n+\frac12}-\partial_tu^{n+\frac12},\partial_t\eta^{n+\frac12})\\=&\frac12(\nabla\eta^{n+\frac12},\nabla\partial_t\eta^{n+\frac12})+(V\eta^{n+\frac12},\partial_t\eta^{n+\frac12}).\end{aligned} \tag{89}$$

Notice

$$\frac{1}{2\tau}(\|\nabla\eta^{n+1}\|^2-\|\nabla\eta^n\|^2)=\mathrm{Re}\{(\nabla\eta^{n+\frac12},\nabla\partial_t\eta^{n+\frac12})\}.$$

Comparing the real parts of (89), we get

$$\begin{aligned}\frac{1}{4\tau}(\|\nabla\eta^{n+1}\|^2-\|\nabla\eta^n\|^2)=&\mathrm{Im}\{(\partial_t\rho^{n+\frac12},\partial_t\eta^{n+\frac12})+(u_t^{n+\frac12}-\partial_tu^{n+\frac12},\partial_t\eta^{n+\frac12})\}\\&-\mathrm{Re}\{(V\eta^{n+\frac12},\partial_t\eta^{n+\frac12})\},\end{aligned}$$

that is,

$$\|\nabla\eta^{n+1}\|^2-\|\nabla\eta^n\|^2=4\tau\mathrm{Im}\{(\partial_t\rho^{n+\frac{1}{2}},\partial_t\eta^{n+\frac{1}{2}})+(u_t^{n+\frac{1}{2}}-\partial_t u^{n+\frac{1}{2}},\partial_t\eta^{n+\frac{1}{2}})\}$$
$$-2V(\|\eta^{n+1}\|^2-\|\eta^n\|^2). \tag{90}$$

Summing up for n in (90) and combining (65), we have

$$\|\nabla\eta^n\|^2\leqslant C\sum_{j=0}^{n-1}\|\partial_t\rho^{j+\frac{1}{2}}\|\|\eta^{j+1}-\eta^j\|$$
$$+C\sum_{j=0}^{n-1}\|u_t^{j+\frac{1}{2}}-\partial_t u^{j+\frac{1}{2}}\|\|\eta^{j+1}-\eta^j\|+C\|\eta^n\|^2. \tag{91}$$

Substituting (61), (66), (62), and (55) into (91), we can obtain

$$\|\nabla\eta^n\|^2\leqslant(Ch^{k+1}+C\tau^2)^2,$$

that is,

$$\|\nabla\eta^n\|\leqslant Ch^{k+1}+C\tau^2,$$

which completes the proof.

Similar to Theorem 3, we can obtain the following result.

Theorem 6 *Assume that $u(\boldsymbol{x},t)$ is the solution to the problem* (2), *and the function series $U^n(\boldsymbol{x})$ is the solution to the problem* (54). *Then, we have the global superconvergence estimate*

$$\|u^n-\Pi_{2h}^{2k}U^n\|_1\leqslant Ch^{k+1}+\tau^2, \tag{92}$$

where Π_{2h}^{2k} is the interpolation post-processing operator.

6 Numerical examples

In this section, we carry out some numerical examples with $k=1$ and $k=2$ to demonstrate the validity of the theoretical analysis.

Example 1 We consider the following linear Schrödinger equation:

$$\begin{cases} \mathrm{i}u_t(\boldsymbol{x},t)=-\dfrac{1}{2}\Delta u(\boldsymbol{x},t)+u(\boldsymbol{x},t)+f(\boldsymbol{x},t) \quad \text{in} \quad \Omega\times[0,1], \\ u(\boldsymbol{x},t)=0 \quad \text{on} \quad \partial\Omega\times[0,1], \\ u(\boldsymbol{x},0)=u_0(\boldsymbol{x}) \quad \text{in} \quad \Omega, \end{cases} \tag{93}$$

where $\Omega=[0,1]\times[0,1]$, and let the function $f(\boldsymbol{x},t)$ be chosen that

$$u(x,y,t)=\mathrm{e}^t(1+\mathrm{i})(1-x)(1-y)\sin x\sin y$$

is the exact solution.

We have solved the Schrödinger equation on the uniformly rectangular meshes with the mesh size h by the bilinear finite element. First, we calculate the errors with fixing $\tau=10^{-4}$ by varying h. The error results are presented in Tables 1–4, where Order_1, Order_2, Order_3, and Order_4 denote the convergence orders of $\|u_I-U^n\|$, $\|u-U^n\|_1$, $\|u_I-U^n\|_1$, and $\|u-\Pi_{2h}^2U^n\|_1$, respectively. Moreover, we have shown convergence orders by slopes in Figs. 2–5. Results in all tables show $O(h)$ in $\|u-U^n\|_1$, and $O(h^2)$ convergence rate clearly in $\|u_I-U^n\|$, $\|u_I-U^n\|_1$, and $\|u-\Pi_{2h}^2U^n\|_1$.

Table 1 Numerical results at $t=0.01$ obtained with $\tau=10^{-4}$ in Example 1

Mesh	$\|u_I-U^n\|$	Order$_1$	$\|u-U^n\|_1$	Order$_2$	$\|u_I-U^n\|_1$	Order$_3$	$\|u-\Pi_{2h}^2U^n\|_1$	Order$_4$
$h=1/8$	9.9357×10^{-5}	–	3.3771×10^{-2}	–	6.2778×10^{-4}	–	1.7558×10^{-3}	–
$h=1/16$	2.5160×10^{-5}	1.982	1.6790×10^{-2}	1.008	1.6956×10^{-4}	1.888	4.4138×10^{-4}	1.992
$h=1/32$	6.3085×10^{-6}	1.996	8.3827×10^{-3}	1.002	4.3226×10^{-5}	1.972	1.1028×10^{-4}	2.001
$h=1/64$	1.5782×10^{-6}	1.999	4.1898×10^{-3}	1.001	1.0848×10^{-5}	1.994	2.7565×10^{-5}	2.000

Table 2 Numerical results at $t=0.1$ obtained with $\tau=10^{-4}$ in Example 1

Mesh	$\|u_I-U^n\|$	Order$_1$	$\|u-U^n\|_1$	Order$_2$	$\|u_I-U^n\|_1$	Order$_3$	$\|u-\Pi_{2h}^2U^n\|_1$	Order$_4$
$h=1/8$	7.4107×10^{-4}	–	3.6917×10^{-2}	–	3.6604×10^{-3}	–	4.2636×10^{-3}	–
$h=1/16$	1.8832×10^{-4}	1.976	1.8367×10^{-2}	1.007	9.4003×10^{-4}	1.961	1.0656×10^{-3}	2.001
$h=1/32$	4.7298×10^{-5}	1.993	9.1716×10^{-3}	1.002	2.3603×10^{-4}	1.994	2.6585×10^{-4}	2.003
$h=1/64$	1.1840×10^{-5}	1.998	4.5844×10^{-3}	1.001	5.9199×10^{-5}	1.995	6.6513×10^{-5}	1.999

Table 3 Numerical results at $t=0.5$ obtained with $\tau=10^{-4}$ in Example 1

Mesh	$\|u_I-U^n\|$	Order$_1$	$\|u-U^n\|_1$	Order$_2$	$\|u_I-U^n\|_1$	Order$_3$	$\|u-\Pi_{2h}^2U^n\|_1$	Order$_4$
$h=1/8$	8.1293×10^{-4}	–	5.4966×10^{-2}	–	4.3017×10^{-3}	–	5.2665×10^{-3}	–
$h=1/16$	2.0388×10^{-4}	1.995	2.7386×10^{-2}	1.005	1.0057×10^{-3}	2.097	1.2577×10^{-3}	2.066
$h=1/32$	5.0843×10^{-5}	2.004	1.3681×10^{-2}	1.001	2.4988×10^{-4}	2.009	3.1505×10^{-4}	1.997
$h=1/64$	1.2719×10^{-5}	1.999	6.8388×10^{-3}	1.000	6.2097×10^{-5}	2.009	7.8531×10^{-5}	2.004

Table 4 Numerical results at $t=1.0$ obtained with $\tau=10^{-4}$ in Example 1

Mesh	$\|u_I-U^n\|$	Order$_1$	$\|u-U^n\|_1$	Order$_2$	$\|u_I-U^n\|_1$	Order$_3$	$\|u-\Pi_{2h}^2U^n\|_1$	Order$_4$
$h=1/8$	2.2407×10^{-3}	–	9.0525×10^{-2}	–	1.0416×10^{-2}	–	1.1400×10^{-2}	–
$h=1/16$	5.8743×10^{-4}	1.932	4.5140×10^{-2}	1.004	2.7423×10^{-3}	1.925	2.9351×10^{-3}	1.958
$h=1/32$	1.4809×10^{-4}	1.988	2.2554×10^{-2}	1.001	6.8316×10^{-4}	2.005	7.2953×10^{-4}	2.008
$h=1/64$	3.7118×10^{-5}	1.996	1.1275×10^{-2}	1.000	1.7124×10^{-4}	1.996	1.8269×10^{-4}	1.998

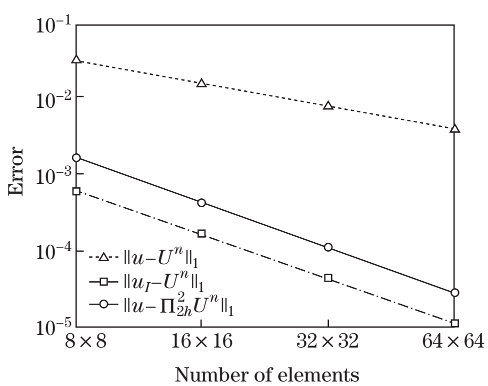

Fig. 2 Log of errors at $t=0.01$ with $\tau=10^{-4}$

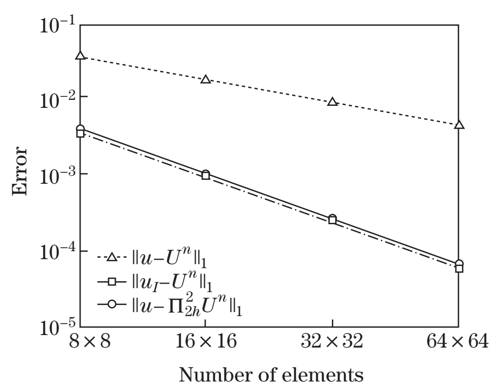

Fig. 3 Log of errors at $t=0.1$ with $\tau=10^{-4}$

To test the convergence rate in terms of τ, we fix the time step $\tau=h$. The error results are shown in Tables 5 and 6. In addition, we also show the convergence orders by slopes in Figs. 6 and 7. Results show the convergence rate $O(\tau^2)$ clearly in $\|u_I-U^n\|$, $\|u_I-U^n\|_1$, and $\|u-\Pi_{2h}^2U^n\|_1$.

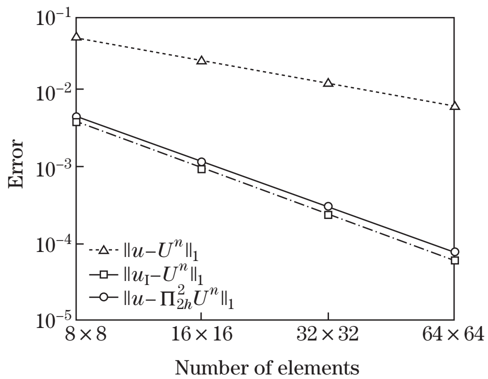

Fig. 4 Log of errors at $t = 0.5$ with $\tau = 10^{-4}$

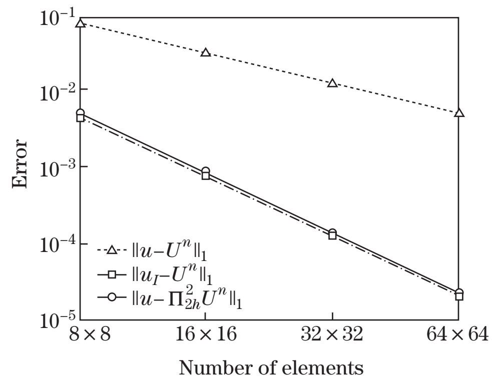

Fig. 5 Log of errors at $t = 1.0$ with $\tau = 10^{-4}$

Table 5 Numerical results at $t = 0.5$ obtained with $\tau = h$ in Example 1

Mesh	$\|u_I - U^n\|$	Order_1	$\|u_I - U^n\|_1$	Order_3	$\|u - \Pi^2_{2h}U^n\|_1$	Order_4
$h = 1/16$	$2.368\,3\times10^{-4}$	–	$1.206\,3\times10^{-3}$	–	$1.438\,3\times10^{-3}$	–
$h = 1/32$	$5.549\,9\times10^{-5}$	2.093	$2.903\,9\times10^{-4}$	2.055	$3.413\,1\times10^{-4}$	2.075
$h = 1/64$	$1.266\,7\times10^{-5}$	2.131	$6.079\,9\times10^{-5}$	2.256	$7.906\,6\times10^{-5}$	2.110
$h = 1/128$	$3.157\,4\times10^{-6}$	2.004	$1.530\,0\times10^{-5}$	1.991	$1.966\,5\times10^{-5}$	2.007

Table 6 Numerical results at $t = 1.0$ obtained with $\tau = h$ in Example 1

Mesh	$\|u_I - U^n\|$	Order_1	$\|u_I - U^n\|_1$	Order_3	$\|u - \Pi^2_{2h}U^n\|_1$	Order_4
$h = 1/16$	$6.684\,9\times10^{-4}$	–	$3.102\,2\times10^{-3}$	–	$3.253\,1\times10^{-3}$	–
$h = 1/32$	$1.531\,9\times10^{-4}$	2.126	$7.081\,4\times10^{-4}$	2.131	$7.523\,1\times10^{-4}$	2.112
$h = 1/64$	$3.746\,2\times10^{-5}$	2.032	$1.743\,2\times10^{-4}$	2.022	$1.856\,1\times10^{-4}$	2.019
$h = 1/128$	$9.282\,6\times10^{-6}$	2.013	$4.273\,5\times10^{-5}$	2.028	$4.563\,1\times10^{-5}$	2.024

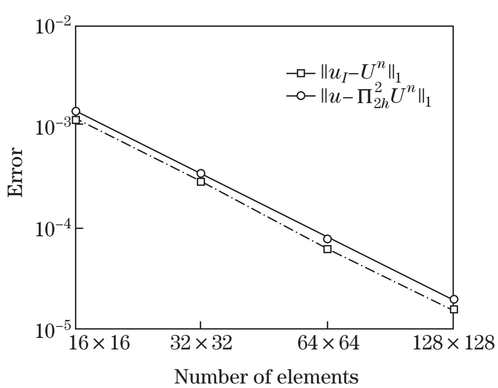

Fig. 6 Log of errors at $t = 0.5$ with $\tau = h$

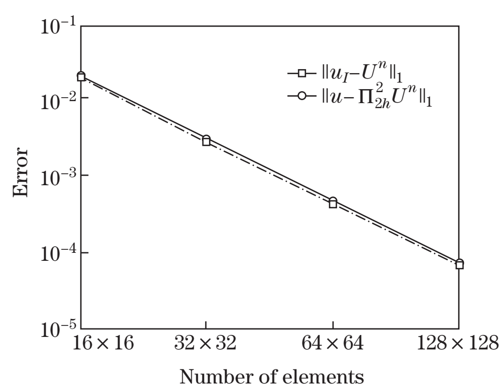

Fig. 7 Log of errors at $t = 1.0$ with $\tau = h$

Example 2 We consider the problem (93) with $\Omega = [-1, 1] \times [-1, 1]$, and function $f(\boldsymbol{x}, t)$ is chosen corresponding to the exact solution

$$u(x, y, t) = \mathrm{e}^t x(1 + x)(1 - x)(1 + y)(1 - y) + \mathrm{i}\mathrm{e}^t x \sin(\pi x) \sin(\pi y).$$

Similarly, we have solved the Schrödinger equation by the bilinear finite element. We calculate the errors with fixing $\tau = 10^{-4}$ by varying h. The error results at the time level $t_n = 0.01, 0.1, 0.5, 1.0$ are presented in Tables 7–10, respectively. Results in all tables show $O(h)$ in $\|u-U^n\|_1$, and $O(h^2)$ convergence rate clearly in $\|u_I-U^n\|$, $\|u_I-U^n\|_1$, and $\|u-\Pi_{2h}^2U^n\|_1$.

Then, we take the time step $\tau = h$. The error results are listed in Tables 11 and 12. Results show the convergence rate $O(\tau^2)$ clearly in $\|u_I-U^n\|$, $\|u_I-U^n\|_1$, and $\|u-\Pi_{2h}^2U^n\|_1$ as well, which are coincident with theoretical results.

The profiles of the exact solution and the numerical solution at $t = 1.0$ on the 64×64 mesh grid are plotted in Figs. 8–11.

Table 7 Numerical results at $t = 0.01$ obtained with $\tau = 10^{-4}$ in Example 2

Mesh	$\|u_I-U^n\|$	Order$_1$	$\|u-U^n\|_1$	Order$_2$	$\|u_I-U^n\|_1$	Order$_3$	$\|u-\Pi_{2h}^2U^n\|_1$	Order$_4$
$h=1/8$	1.3695×10^{-3}	–	4.3513×10^{-1}	–	8.8605×10^{-3}	–	8.3676×10^{-2}	–
$h=1/16$	3.4678×10^{-4}	1.982	2.1675×10^{-1}	1.005	2.2779×10^{-3}	1.960	2.1245×10^{-2}	1.978
$h=1/32$	8.6958×10^{-5}	1.996	1.0827×10^{-1}	1.001	5.7318×10^{-4}	1.991	5.3302×10^{-3}	1.995
$h=1/64$	2.1756×10^{-5}	1.999	5.4123×10^{-2}	1.000	1.4353×10^{-4}	1.998	1.3337×10^{-3}	1.999

Table 8 Numerical results at $t = 0.1$ obtained with $\tau = 10^{-4}$ in Example 2

Mesh	$\|u_I-U^n\|$	Order$_1$	$\|u-U^n\|_1$	Order$_2$	$\|u_I-U^n\|_1$	Order$_3$	$\|u-\Pi_{2h}^2U^n\|_1$	Order$_4$
$h=1/8$	1.2188×10^{-2}	–	4.7595×10^{-1}	–	7.0779×10^{-2}	–	1.1561×10^{-1}	–
$h=1/16$	3.0903×10^{-3}	1.980	2.3714×10^{-1}	1.005	1.7818×10^{-2}	1.990	2.9078×10^{-2}	1.991
$h=1/32$	7.7531×10^{-4}	1.995	1.1847×10^{-1}	1.001	4.4659×10^{-3}	1.996	7.2819×10^{-3}	1.998
$h=1/64$	1.9400×10^{-4}	1.999	5.9220×10^{-2}	1.000	1.1171×10^{-3}	1.999	1.8211×10^{-3}	2.000

Table 9 Numerical results at $t = 0.5$ obtained with $\tau = 10^{-4}$ in Example 2

Mesh	$\|u_I-U^n\|$	Order$_1$	$\|u-U^n\|_1$	Order$_2$	$\|u_I-U^n\|_1$	Order$_3$	$\|u-\Pi_{2h}^2U^n\|_1$	Order$_4$
$h=1/8$	2.0535×10^{-2}	–	7.0896×10^{-1}	–	1.1175×10^{-1}	–	1.7606×10^{-1}	–
$h=1/16$	5.1357×10^{-3}	1.999	3.5363×10^{-1}	1.004	2.7709×10^{-2}	2.012	4.4016×10^{-2}	2.000
$h=1/32$	1.2836×10^{-3}	2.000	1.7671×10^{-1}	1.001	6.9144×10^{-3}	2.003	1.1005×10^{-2}	2.000
$h=1/64$	3.2085×10^{-4}	2.000	8.8343×10^{-2}	1.000	1.7270×10^{-3}	2.001	2.7508×10^{-3}	2.000

Table 10 Numerical results at $t = 1.0$ obtained with $\tau = 10^{-4}$ in Example 2

Mesh	$\|u_I-U^n\|$	Order$_1$	$\|u-U^n\|_1$	Order$_2$	$\|u_I-U^n\|_1$	Order$_3$	$\|u-\Pi_{2h}^2U^n\|_1$	Order$_4$
$h=1/8$	2.1954×10^{-2}	–	1.1672	–	1.2333×10^{-1}	–	2.5572×10^{-1}	–
$h=1/16$	6.0520×10^{-3}	1.859	5.8284×10^{-1}	1.002	3.3824×10^{-2}	1.866	6.5942×10^{-2}	1.955
$h=1/32$	1.5509×10^{-3}	1.964	2.9132×10^{-1}	1.001	8.6926×10^{-3}	1.960	1.6636×10^{-2}	1.987
$h=1/64$	3.9009×10^{-4}	1.991	1.4565×10^{-1}	1.000	2.1879×10^{-3}	1.990	4.1682×10^{-3}	1.997

Table 11 Numerical results $t = 0.5$ obtained with $\tau = h$ in Example 2

Mesh	$\|u_I-U^n\|$	Order$_1$	$\|u_I-U^n\|_1$	Order$_3$	$\|u-\Pi_{2h}^2U^n\|_1$	Order$_4$
$h=1/16$	4.3946×10^{-3}	–	2.3066×10^{-2}	–	4.1306×10^{-2}	–
$h=1/32$	1.2460×10^{-3}	1.818	6.7001×10^{-3}	1.784	1.0876×10^{-2}	1.925
$h=1/64$	3.1896×10^{-4}	1.966	1.7114×10^{-3}	1.969	2.7413×10^{-3}	1.988
$h=1/128$	8.0206×10^{-5}	1.992	4.3034×10^{-4}	1.992	6.8686×10^{-4}	1.997

Table 12 Numerical results at $t = 1.0$ obtained with $\tau = h$ in Example 2

Mesh	$\|u_I - U^n\|$	Order$_1$	$\|u_I - U^n\|_1$	Order$_3$	$\|u - \Pi_{2h}^2 U^n\|_1$	Order$_4$
$h = 1/16$	7.2718×10^{-3}	–	4.1379×10^{-2}	–	7.0050×10^{-2}	–
$h = 1/32$	1.6874×10^{-3}	2.108	9.5410×10^{-3}	2.117	1.7083×10^{-2}	2.036
$h = 1/64$	4.0062×10^{-4}	2.075	2.2545×10^{-3}	2.081	4.2027×10^{-3}	2.023
$h = 1/128$	9.8441×10^{-5}	2.025	5.5237×10^{-4}	2.029	1.0449×10^{-3}	2.008

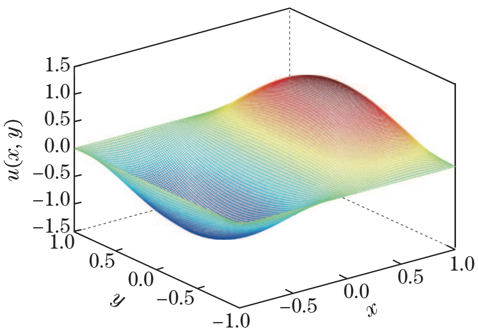

Fig. 8 Real parts of exact solution (color online)

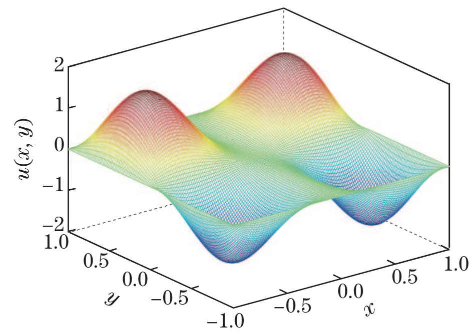

Fig. 9 Imaginary parts of exact solution (color online)

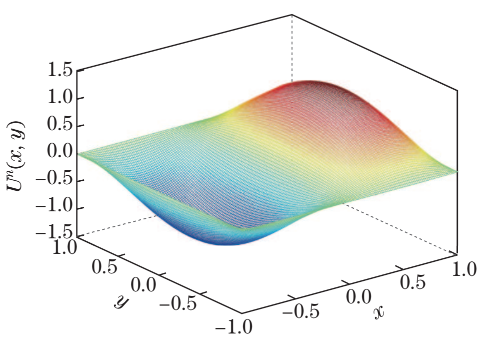

Fig. 10 Real parts of numerical solution (color online)

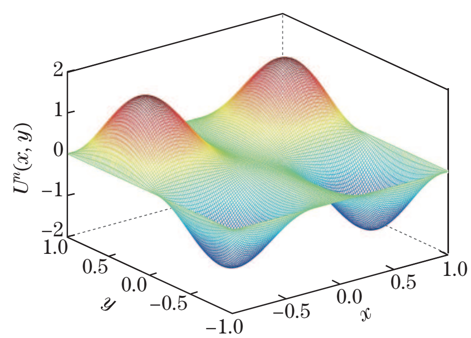

Fig. 11 Imaginary parts of numerical solution (color online)

Example 3 We consider the problem (93) with $\Omega = [-1, 1] \times [-1, 1]$, and function $f(\boldsymbol{x}, t)$ is chosen corresponding to the same exact solution with Example 2.

The domain Ω is uniformly divided into families Γ_h of quadrilaterals with mesh size h, and $V^{h,2}$ is the biquadratic rectangular element space defined on Γ_h. The Schrödinger equation is solved by the biquadratic rectangular element. We calculate the errors with fixing $\tau = 10^{-3}$ by varying h. The error results at time level $t_n = 0.1, 0.2, 0.5, 1.0$ are presented in Tables 13–16, respectively. Results in all tables also show $O(h^2)$ in $\|u - U^n\|_1$, and $O(h^3)$ convergence rate clearly in $\|u - U^n\|$ and $\|u_I - U^n\|_1$, which are consistent with our theoretical analysis. In addition, the results show $O(h^4)$ in $\|u_I - U^n\|$. When $k \geqslant 2$, there is the superclose property also in the L^2 norm between the numerical solution with the interpolant of exact solution.

Table 13 Numerical results at $t = 0.1$ obtained with $\tau = 10^{-3}$

Mesh	$\|u - U^n\|$	Order	$\|u_I - U^n\|$	Order$_1$	$\|u - U^n\|_1$	Order$_2$	$\|u_I - U^n\|_1$	Order$_3$
$h = 1/4$	2.8434×10^{-3}	–	3.0951×10^{-4}	–	9.0911×10^{-2}	–	4.9860×10^{-3}	–
$h = 1/8$	3.6930×10^{-4}	2.945	2.0733×10^{-5}	3.900	2.3106×10^{-2}	1.976	6.7424×10^{-4}	2.887
$h = 1/16$	4.6680×10^{-5}	2.984	1.2780×10^{-6}	4.020	5.7986×10^{-3}	1.995	7.8974×10^{-5}	3.094
$h = 1/32$	5.8523×10^{-6}	2.996	7.2122×10^{-8}	4.147	1.4510×10^{-3}	1.999	3.9969×10^{-6}	4.304

Table 14 Numerical results at $t = 0.2$ obtained with $\tau = 10^{-3}$

Mesh	$\|u - U^n\|$	Order	$\|u_I - U^n\|$	Order$_1$	$\|u - U^n\|_1$	Order$_2$	$\|u_I - U^n\|_1$	Order$_3$
$h = 1/4$	3.0812×10^{-3}	–	4.3760×10^{-4}	–	1.0047×10^{-1}	–	7.1099×10^{-3}	–
$h = 1/8$	4.0784×10^{-4}	2.917	2.6292×10^{-5}	4.057	2.5536×10^{-2}	1.976	6.8993×10^{-4}	3.365
$h = 1/16$	5.1558×10^{-5}	2.984	1.6869×10^{-6}	3.962	6.4084×10^{-3}	1.995	9.2336×10^{-5}	2.902
$h = 1/32$	6.4665×10^{-6}	2.995	1.0013×10^{-7}	4.075	1.6036×10^{-3}	1.999	7.0384×10^{-6}	3.714

Table 15 Numerical results at $t = 0.5$ obtained with $\tau = 10^{-3}$

Mesh	$\|u - U^n\|$	Order	$\|u_I - U^n\|$	Order$_1$	$\|u - U^n\|_1$	Order$_2$	$\|u_I - U^n\|_1$	Order$_3$
$h = 1/4$	4.2589×10^{-3}	–	4.3852×10^{-4}	–	1.3557×10^{-1}	–	5.2243×10^{-3}	–
$h = 1/8$	5.5136×10^{-4}	2.949	2.9882×10^{-5}	3.875	3.4468×10^{-2}	1.976	7.9431×10^{-4}	2.718
$h = 1/16$	6.9627×10^{-5}	2.985	1.9090×10^{-6}	3.968	8.6503×10^{-3}	1.994	1.0669×10^{-4}	2.896
$h = 1/32$	8.7270×10^{-6}	2.996	1.2394×10^{-7}	3.945	2.1646×10^{-3}	1.999	1.4431×10^{-5}	2.886

Table 16 Numerical results at $t = 1.0$ obtained with $\tau = 10^{-3}$

Mesh	$\|u - U^n\|$	Order	$\|u_I - U^n\|$	Order$_1$	$\|u - U^n\|_1$	Order$_2$	$\|u_I - U^n\|_1$	Order$_3$
$h = 1/4$	6.9955×10^{-3}	–	6.2494×10^{-4}	–	2.2348×10^{-1}	–	1.0268×10^{-2}	–
$h = 1/8$	9.0956×10^{-4}	2.943	4.0484×10^{-5}	3.948	5.6826×10^{-2}	1.976	1.2887×10^{-3}	2.994
$h = 1/16$	1.1487×10^{-4}	2.985	2.4265×10^{-6}	4.060	1.4262×10^{-2}	1.994	1.3386×10^{-4}	3.267
$h = 1/32$	1.4392×10^{-5}	2.997	1.5049×10^{-7}	4.011	3.5688×10^{-3}	1.999	1.4348×10^{-5}	3.222

7 Conclusions

In this paper, we consider a two-dimensional time-dependent linear Schrödinger equation with the finite element method. We present the finite element semi-discrete scheme and the Crank-Nicolson fully discrete scheme in the rectangular Lagrange type finite element space of order k. We also obtain the superconvergence result in the H^1 norm by use of the elliptic projection in the semi-discrete scheme and the fully discrete scheme, respectively. Some numerical examples with the order $k = 1$ and $k = 2$ are provided to partly verify our theoretical results. In the future, we shall try to study the problem of superconvergence in the L^2 norm for the two-dimensional time-dependent Schrödinger equation and the superconvergence in the H^1 norm for the three-dimensional Schrödinger equation with the finite element method.

Acknowledgements We would like to thank anonymous referees for their insightful comments that improved this paper.

References

[1] BAO, W. Z., JIN, S., and MARKOWICH, P. A. Numerical study of time-splitting spectral discretizations of nonlinear Schrödinger equations in the semiclassical regimes. *SIAM Journal on Scientific Computing*, **25**(1), 27–64 (2003)

[2] FEIT, M. D., FLECK, J. A., and STEIGER, A. Solution of the Schrödinger equation by a spectral method. *Journal of Computational Physics*, **47**, 412–433 (1982)

[3] AKRIVIS, G. D. Finite difference discretization of the cubic Schrödinger equation. *IMA Journal of Numerical Analysis*, **13**(1), 115–124 (1993)

[4] BAO, W. Z. and CAI, Y. Y. Uniform error estimates of finite difference methods for the nonlinear Schrödinger equation with wave operator. *SIAM Journal on Numerical Analysis*, **50**(2), 492–521 (2012)

[5] HAN, H. D., JIN, J. C., and WU, X. N. A finite-difference method for the one-dimensional time-dependent Schrödinger equation on unbounded domain. *Computers and Mathematics with Applications*, **50**(8), 1345–1362 (2005)

[6] AKRIVIS, G. D., DOUGALIS, V. A., and KARAKASHIAN, O. A. On fully discrete Galerkin methods of second-order temporal accuracy for the nonlinear Schrödinger equation. *Numerische Mathematik*, **59**(1), 31–53 (1991)

[7] ANTONOPOULOU, D. C., KARALI, G. D., PLEXOUSAKIS, M., and ZOURARIS, G. E. Crank-Nicolson finite element discretizations for a two-dimensional linear Schrödinger-type equation posed in a noncylindrical domain. *Mathematics of Computation*, **84**(294), 1571–1598 (2015)

[8] JIN, J. C. and WU, X. N. Convergence of a finite element scheme for the two-dimensional time-dependent Schrödinger equation in a long strip. *Journal of Computational and Applied Mathematics*, **234**(3), 777–793 (2010)

[9] KYZA, I. A posteriori error analysis for the Crank-Nicolson method for linear Schrödinger equations. *ESAIM Mathematical Modelling and Numerical Analysis*, **45**(4), 761–778 (2011)

[10] LEE, H. Y. Fully discrete methods for the nonlinear Schrödinger equation. *Computers and Mathematics with Applications*, **28**(6), 9–24 (1994)

[11] TANG, Q., CHEN, C. M., and LIU, L. H. Space-time finite element method for Schrödinger equation and its conservation. *Applied Mathematics and Mechanics* (*English Edition*), **27**(3), 335–340 (2006) https://doi.org/10.1007/s10483-006-0308-z

[12] WANG, J. Y. and HUANG Y. Q. Fully discrete Galerkin finite element method for the cubic nonlinear Schrödinger equation. *Numerical Mathematics*: *Theory*, *Methods and Applications*, **10**(3), 670–687 (2017)

[13] ANTONOPOULOU, D. C. and PLEXOUSAKIS, M. Discontinuous Galerkin methods for the linear Schrödinger equation in non-cylindrical domains. *Numerische Mathematik*, **115**(4), 585–608 (2010)

[14] KARAKASHIAN, O. A. and MAKRIDAKIS C. A space-time finite element method for the nonlinear Schrödinger equation: the discontinuous Galerkin method. *Mathematics of Computation*, **67**(222), 479–499 (1998)

[15] LU, W. Y., HUANG, Y. Q., and LIU, H. L. Mass preserving discontinuous Galerkin methods for Schrödinger equations. *Journal of Computational Physics*, **282**, 210–226 (2015)

[16] GUO, L. and XU, Y. Energy conserving local discontinuous Galerkin methods for the nonlinear Schrödinger equation with wave operator. *Journal of Scientific Computing*, **65**(2), 622–647 (2015)

[17] WANG, W. and SHU, C. W. The WKB local discontinuous Galerkin method for the simulation of Schrödinger equation in a resonant tunneling diode. *Journal of Scientific Computing*, **40**(1-3), 360–374 (2009)

[18] XU, Y. and SHU, C. W. Local discontinuous Galerkin methods for nonlinear Schrödinger equations. *Journal of Computational Physics*, **205**, 72–97 (2005)

[19] CHEN, C. M. and HUANG Y. Q. *High Accuracy Theory of Finite Element Methods* (in Chinese), Hunan Science Press, Changsha, 235–248 (1995)

[20] LIN, Q. and YAN, N. N. *Construction and Analysis of High Efficient Finite Elements* (in Chinese), Hebei University Press, Baoding, 175–185 (1996)

[21] WAHLBIN, L. B. *Superconvergence in Galerkin Finite Element Methods*, Springer, Berlin, 48–64 (1995)

[22] YAN, N. N. *Superconvergence Analysis and a Posteriori Error Estimation in Finite Element Methods*, Science Press, Beijing, 35–156 (2008)

[23] ARNOLD, D. N., DOUGLAS, J., Jr., and THOMÉE, V. Superconvergence of a finite element approximation to the solution of a Sobolev equation in a single space variable. *Mathematics of Computation*, **36**(153), 53–63 (1981)

[24] CHEN, C. M. and HU, S. F. The highest order superconvergence for bi-k degree rectangular elements at nodes: a proof of $2k$-conjecture. *Mathematics of Computation*, **82**(283), 1337–1355 (2013)

[25] CHEN, Y. P. Superconvergence of mixed finite element methods for optimal control problems. *Mathematics of Computation*, **77**(263), 1269–1291 (2008)

[26] CHEN, Y. P., HUANG, Y. Q., LIU, W. B., and YAN, N. N. Error estimates and superconvergence of mixed finite element methods for convex optimal control problems. *Journal of Scientific Computing*, **42**(3), 382–403 (2010)

[27] HUANG, Y. Q., LI, J. C., WU, C., and YANG, W. Superconvergence analysis for linear tetrahedral edge elements. *Journal of Scientific Computing*, **62**(1), 122–145 (2015)

[28] HUANG, Y. Q., YANG, W., and YI, N. Y. A posteriori error estimate based on the explicit polynomial recovery. *Natural Science Journal of Xiangtan University*, **33**(3), 1–12 (2011)

[29] LIN, Q. and ZHOU, J. M. Superconvergence in high-order Galerkin finite element methods. *Computer Methods in Applied Mechanics and Engineering*, **196**(37), 3779–3784 (2007)

[30] SHI, D. Y. and PEI, L. F. Superconvergence of nonconforming finite element penalty scheme for Stokes problem using L^2 projection method. *Applied Mathematics and Mechanics* (*English Edition*), **34**(7), 861–874 (2013) https://doi.org/10.1007/s10483-013-1713-x

[31] WHEELER, M. F. and WHITEMAN, J. R. Superconvergence of recovered gradients of discrete time/piecewise linear Galerkin approximations for linear and nonlinear parabolic problems. *Numerical Methods for Partial Differential Equations*, **10**(3), 271–294 (1994)

[32] LIN, Q. and LIU, X. Q. Global superconvergence estimates of finite element method for Schrödinger equation. *Journal of Computational Mathematics*, **16**(6), 521–526 (1998)

[33] SHI, D. Y., WANG, P. L., and ZHAO, Y. M. Superconvergence analysis of anisotropic linear triangular finite element for nonlinear Schrödinger equation. *Applied Mathematics Letters*, **38**, 129–134 (2014)

[34] TIAN, Z. K., CHEN, Y. P., and WANG J. Y. Superconvergence analysis of bilinear finite element for the nonlinear Schrödinger equation on the rectangular mesh. *Advances in Applied Mathematics and Mechanics*, **10**(2), 468–484 (2018)

[35] WANG, J. Y., HUANG, Y. Q., TIAN, Z. K., and ZHOU, J. Superconvergence analysis of finite element method for the time-dependent Schrödinger equation. *Computers and Mathematics with Applications*, **71**(10), 1960–1972 (2016)

[36] ZHOU, L. L., XU, Y., ZHANG, Z. M., and CAO, W. X. Superconvergence of local discontinuous Galerkin method for one-dimensional linear Schrödinger equations. *Journal of Scientific Computing*, **73**(2/3), 1290–1315 (2017)

[37] HU, H. L., CHEN, C. M., and PAN, K. J. Time-extrapolation algorithm (TEA) for linear parabolic problems. *Journal of Computational Mathematics*, **32**(2), 183–194 (2014)